Evaluation of 3D printed PCL/PLGA/β-TCP versus collagen membranes for guided bone regeneration in a beagle implant model

To cite this article: J-Y Won *et al* 2016 *Biomed. Mater.* **11** 055013

Biomedical Materials

OPEN ACCESS

PAPER

Evaluation of 3D printed PCL/PLGA/β-TCP versus collagen membranes for guided bone regeneration in a beagle implant model

J-Y Won[2,5], C-Y Park[1,5], J-H Bae[1,5], G Ahn[2], C Kim[2], D-H Lim[3], D-W Cho[4], W-S Yun[3], J-H Shim[3] and J-B Huh[1]

[1] Department of Prosthodontics, Dental Research Institute, Institute of Translation Dental Science, School of Dentistry, Pusan National University, YangSan, Gyeongnam 676-870, Korea
[2] Research Institute, T&R Biofab Co. Ltd, 237 Sangidaehak-Ro, Siheung-Si, Gyeonggi-Do 15073, Korea
[3] Department of Mechanical Engineering, Korea Polytechnic University, 237 Sangidaehak-Ro, Siheung-Si, Gyeonggi-Do 15073, Korea
[4] Department of Mechanical Engineering, Pohang University of Science and Technology (POSTECH), 77 Cheong-Am Ro, Nam-gu, Pohang, Kyungbuk 37673, Korea
[5] These authors contributed equally to this work

E-mail: happyshim@kpu.ac.kr (J-H Shim) and huhjb@pusan.ac.kr (J-B Huh)

RECEIVED
20 May 2016

REVISED
10 August 2016

ACCEPTED FOR PUBLICATION
25 August 2016

PUBLISHED
7 October 2016

Keywords: PCL/PLGA/β-TCP, 3D printing, collagen, guided bone regeneration, osteointegration, beagle dog

Abstract

Here, we compared 3D-printed polycaprolactone/poly(lactic-co-glycolic acid)/β-tricalcium phosphate (PCL/PLGA/β-TCP) membranes with the widely used collagen membranes for guided bone regeneration (GBR) in beagle implant models. For mechanical property comparison in dry and wet conditions and cytocompatibility determination, we analyzed the rate and pattern of cell proliferation of seeded fibroblasts and preosteoblasts using the cell counting kit-8 assay and scanning electron microscopy. Osteogenic differentiation was verified using alizarin red S staining. At 8 weeks following implantation *in vivo* using beagle dogs, computed tomography and histological analyses were performed after sacrifice. Cell proliferation rates *in vitro* indicated that early cell attachment was higher in collagen than in PCL/PLGA/β-TCP membranes; however, the difference subsided by day 7. Similar outcomes were found for osteogenic differentiation, with approximately 2.5 times greater staining in collagen than PCL/PLGA/β-TCP, but without significant difference by day 14. *In vivo*, bone regeneration in the defect area, represented by new bone formation and bone-to-implant contact, paralleled those associated with collagen membranes. However, tensile testing revealed that whereas the PCL/PLGA/β-TCP membrane mechanical properties were conserved in both wet and dry states, the tensile property of collagen was reduced by 99% under wet conditions. Our results demonstrate *in vitro* and *in vivo* that PCL/PLGA/β-TCP membranes have similar levels of biocompatibility and bone regeneration as collagen membranes. In particular, considering that GBR is always applied to a wet environment (e.g. blood, saliva), we demonstrated that PCL/PLGA/β-TCP membranes maintained their form more reliably than collagen membranes in a wet setting, confirming their appropriateness as a GBR membrane.

1. Introduction

Adequate bone volume is critical for the successful outcome of dental implants and prosthetic superstructures and to ensure satisfactory predictable aesthetics and long-term prognoses [1, 2]. To enhance the bone volume in the jaw, various methods such as distraction osteogenesis [3], osteoinduction [4], osteoconduction [5], and guided bone regeneration (GBR) [6, 7] have been introduced. Among these methods, GBR, a surgical procedure that uses a barrier membrane with or without grafting materials, has been recognized as the method that yields the most predictable results for new bone regeneration in peri-implant bone defect sites [8, 9].

During the GBR procedure, the bone defect is separated from the surrounding connective tissues to prepare a space for new bone formation. The barrier membrane plays important roles during this procedure [9, 10] and is required to exhibit properties such as

biocompatibility, cell occlusivity, tissue integration, space maintenance, and manageability [11]. To date, both non-resorbable and resorbable commercially available membranes with unique properties have been used in the clinic because they have met consumer needs as GBR membranes [12, 13]. Most recently, resorbable membranes have been preferentially utilized because the non-resorbable forms inevitably require a surgical procedure for membrane removal, which can cause further patient discomfort, risk of tissue damage, and additional costs and duration of treatments [13, 14]. Moreover, non-resorbable membranes carry limitations such as a high membrane exposure rate and infection problems; thus, it is primarily used for specific indications in the form of titanium-reinforced expanded-polytetrafluoroethylene (e-PTFE) or as a titanium-mesh [1, 15].

In comparison, the collagen membrane, which is widely used as a representative resorbable GBR membrane, is mechanically malleable and adaptable, exhibiting excellent manipulability [16, 17]. Owing to its collagen property, it has advantages such as a hemostatic function, early wound stabilization, and semipermeablity [18], but it also has drawbacks such as unfavorable mechanical properties [19] and inadequate barrier stability over time [20–22]. Accordingly, studies on synthetic bioresorbable materials have been conducted for the fabrication of form-stable resorbable GBR membranes with a sufficient degradation rate [13, 23]. Bioresorbable materials such as polyglycolides (PGAs), polylactides (PLAs), and copolymers have been used for medical purposes [24]. The synthetic membranes prepared using those materials have been shown to be sufficiently biocompatible and biodegradable to also be used as barrier membranes [25–29].

Bioresorbable synthetic polymers are often used in tissue-engineering scaffolds that can be prepared through foaming/particulate leaching, phase separation, freeze-drying, and electrospinning [30]. However, these conventional fabrication techniques utilize toxic solvents that adversely affect cells and tissues if not completely removed. Furthermore, it is difficult to adjust the thickness, pore size, or external shape of the fabricated scaffold, and to maintain the architectural consistency [30, 31].

In contrast, three dimensional (3D) structures can be prepared without the aforementioned difficulties using the 3D printing method, which is based on computer-aided design/computer-aided manufacturing (CAD/CAM) and layer-by-layer processes [32, 33]. In particular, the multi-head deposition system (MHDS), an advanced type of extrusion-based 3D printing technology, has four dispensing heads for preparing hybrid scaffolds containing multiple biomaterials, and can prepare 3D microstructures precisely within a short time [34, 35]. For example, Shim *et al* [31] fabricated thin-membrane-type scaffolds using MHDS by blending polycaprolactone (PCL), poly(lactic-co-glycolic acid) (PLGA), and beta-tricalcium phosphate (β-TCP), and confirmed that the PCL/PLGA/β-TCP membrane prepared using the 3D printing technology promoted appropriate bone-formation in a rabbit calvaria bone-defect model [36–38]. This bioresorbable PCL/PLGA/β-TCP membrane has the biological and mechanical advantages of both PCL and PLGA, as well as the osteoconductivity of TCP. In addition, it can be prepared with diverse thicknesses and pore sizes via the 3D printing technology, and can be effectively used as a GBR membrane for peri-implant bone defects [39]. In a further Shim *et al* study [40], GBR procedures were conducted at the buccal open defects surrounding implants in the mandible of beagle dogs in designed clinical situations, and the bone generation effects of the PCL/PLGA/β-TCP membrane were compared with those of the non-resorbable titanium membrane. The results of this study confirmed that the PCL/PLGA/β-TCP membrane promoted sufficient new bone formation to serve as a GBR membrane [40].

In the current study, the bone regeneration ability of the 3D-printed PCL/PLGA/β-TCP membrane was evaluated and compared with that of the collagen membrane, a widely used resorbable membrane, during the GBR procedure for peri-implant bone defects in the beagle mandible.

2. Experimental section

2.1. PCL/PLGA/β-TCP membrane generation using 3D printing technology

2.1.1. Preparation of blended PCL/PLGA/β-TCP

Collagen membrane (GENOSS, Suwon, Korea) and PCL/PLGA/β-TCP membrane were used as barrier membranes. The PCL/PLGA/β-TCP membrane was prepared using the thermal melting process by mixing PCL (19561-500G, 43 000–50 000 Mw; Polysciences Inc., Warrington, PA, USA), PLGA (430471-5G, 50 000–75 000 Mw; Sigma-Aldrich, St. Louis, MO, USA), and β-TCP (average diameter: 100 nm, Berkeley Advanced Biomaterials Inc., Berkeley, CA, USA). Briefly, PCL (0.4 g) and PLGA (0.5 g) granules were melted and mixed in a glass container for 10 min at 130 °C, and powder-type β-TCP (0.1 g) was added to the dissolved PCL and PLGA mixture, which was further mixed for five min. Then the PCL/PLGA/β-TCP mixture was put into the 10 ml steel syringe of the multi-head deposition system (MHDS) and maintained at 135 °C for dispensing.

2.1.2. Fabrication of PCL/PLGA/β-TCP membranes

The MHDS, an extrusion-based 3D printing system used to prepare the PCL/PLGA/β-TCP membrane, was composed of four heads that could control the temperature, pneumatic pressure, and motion during extrusion. The system could simultaneously prepare four membranes [31]. Blended PCL/PLGA/β-TCP fibers were dispensed from the steel nozzle of the head at 135 °C and 650 kPa. In total, three layers were stacked to fabricate PCL/PLGA/β-TCP membranes using the layer-by-layer process. The PCL/PLGA/β-TCP membrane

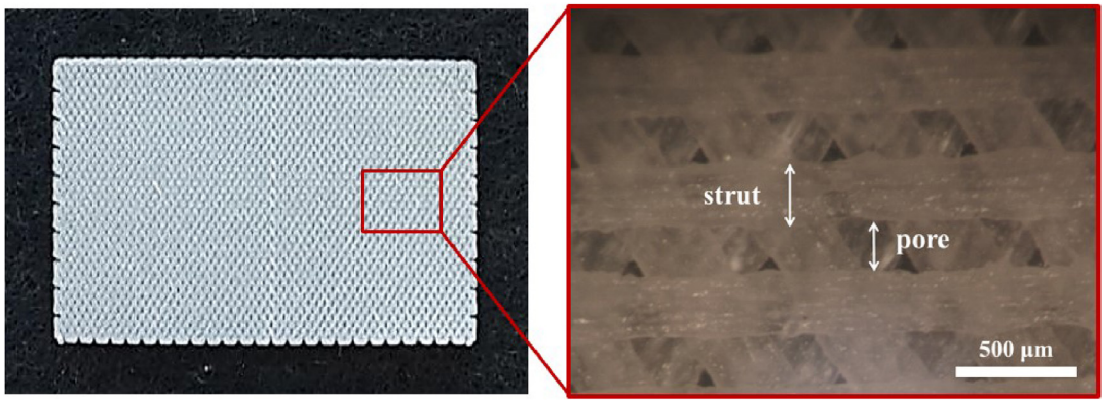

Figure 1. Photographs of the PCL/PLGA/β-TCP membrane.

had a 3D-multilayer mesh-type structure similar to that of the resorbable collagen membrane. The 3D-printed membranes included a triangular pore structure. The overall dimensions were 30 mm × 20 mm × 0.25 mm (figure 1). The width of the strut was 300 μm and the pore size was 200 μm. Therefore, the calculated porosity was approximately 40%.

2.1.3. Mechanical testing of collagen and PCL/PLGA/β-TCP membranes

A membrane-type specimen for a mechanical tensile test was fabricated using the 3D printing system. The experiment condition was based on ISO527 (Tensile test on plastics) and the dimensions of the specimen were determined according to Specimen Type 4 of ISO527-3. The tensile test of the membranes was performed using a single-column tensile test machine (Model 3345, Instron Co., Norwood, MA, USA) under dry and wet (soaking the membranes in a medium for 18 h) membrane conditions. The overall dimensions of the collagen and PCL/PLGA/β-TCP membranes were 30 mm × 10 mm × 0.3 mm. For the PCL/PLGA/β-TCP membrane, the printed strut size was 300 μm, and the membrane pore size was 200 μm. The load and displacement were monitored at a constant cross-head speed of 5 mm min^{-1}.

2.2. *In vitro* analyses

2.2.1. Cell culture and proliferation assay

Mouse fibroblasts (NIH3T3, ATCC #CRL-1658) and preosteoblasts (MC3T3-E1, ATCC #CRL-2593) were maintained in Dulbecco modified Eagle's medium (DMEM) and α-MEM containing 10% fetal bovine serum (FBS) and 1% penicillin and streptomycin (all from Invitrogen, Carlsbad, CA, USA). For cell seeding on the membranes, all membranes (10 mm × 10 mm × 0.3 mm) were pre-wetted in culture medium for 2 h and then irradiated under UV for 30 min. Subsequently, 3 × 10^5 cells were seeded on each membrane and the rates of proliferation on the membrane were analyzed via a Cell Counting Kit-8 (CCK-8, Dojindo, Rockville, MD, USA) on day 2, 4, and 7.

2.2.2. Osteogenic differentiation and Alizarin red staining

The MC3T3-E1-seeded membranes were incubated in culture medium for 3 d, which was then replaced with osteogenic medium composed of α-MEM plus 20% FBS, 10-8 M dexamethasone, 0.2 mM ascorbic acid, 10 mM β-glycerol phosphate (all from Sigma-Aldrich) and 1% penicillin/streptomycin. The membranes were fixed with 4% paraformaldehyde on day 7 and 14, then stained with alizarin red to measure calcium deposition. For the quantification of staining, membranes were soaked in 10% cetylpyridinium chloride for 10 min at room temperature and the optical density was measured at 570 nm using a microplate reader (Epoch, BioTek, Winooski, VT, USA).

2.2.3. Scanning electron microscopy (SEM)

To assess the morphology of the membrane surface alone or following cell seeding, we performed SEM a using high resolution SEM (HR-SEM) with acceleration voltage of 10 kV (FEI, Nova NanoSEM 450) as previously described [40].

2.3. *In vivo* analyses

2.3.1. Experimental animals

Three systemically healthy male beagle dogs aged 18 months and weighing approximately 10 kg were used in this study. All the experimental animals were fed a soft food diet to preserve their dentition with a healthy periodontium. The animal selection and management as well as the surgical procedures were approved by the Ethics Committee on Animal Experimentation of Chonnam National University (CNU IACUC-TB-2013-10). All the experiments were performed at the animal dental laboratory accredited by the Chonnam National University Animal Hospital.

2.3.2. Experiment design

A total of 12 implants (INNO Implant, Cowelmedi, Busan, Korea), 3.0 mm in diameter and 6.0 mm in length, were bilaterally placed in healed extraction sites (below). A total of four peri-implant dehiscence defects were observed per animal, and the following two therapeutic methods were randomly applied:

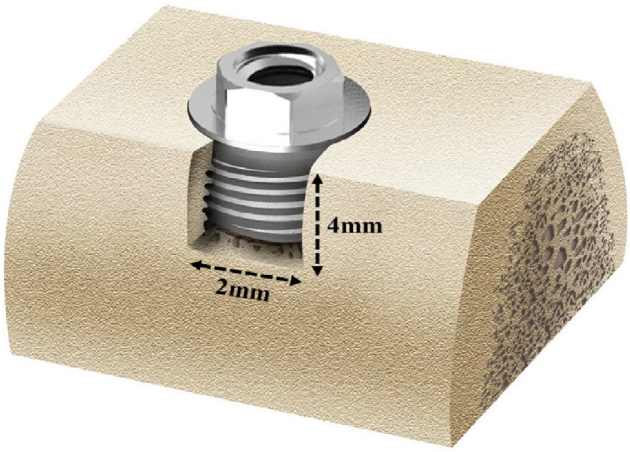

Figure 2. Schematic diagram of the peri-implant defect model. The implant (3.0 mm × 6.0 mm) was inserted in a standardized defect, 4 mm in height and 2 mm in width.

- Collagen group: Collagen Membrane (GENOSS, Suwon, Korea) with a deproteinized bovine bone grafting material (Bio-Oss, Geistlich Biomaterials, Wolhusen, Switzerland).
- PCL/PLGA/β-TCP group: PCL/PLGA/β-TCP membrane with a deproteinized bovine bone grafting material (Bio-Oss).

2.3.3. Surgical procedures

The first surgery was performed to extract the second and fourth premolars (P2 and P4) under general anesthesia induced by intravenous injection of atropine (0.05 mg kg^{-1} IV; Dai Han Pharm Co., Seoul, Korea) and intramuscular injection of a combination of xylazine (Rompun, Bayer Korea Co., Seoul, Korea), followed by inhalation of anesthesia with isoflurane (Choongwae Co., Seoul, Korea). At the surgical sites, dental infiltration anesthesia was used with 1 ml 2% lidocaine HCL and 1:100 000 epinephrine (Yu-Han Co., Gunpo, Korea). The targeted premolars were bilaterally extracted. The extraction site was sutured with 4-0 nylon (Mersilk, Ethicon Co., Livingston, UK) for healing. Oral prophylaxis was performed on the remaining teeth. The stitches were removed after 10 d, and the extraction sites were allowed to heal.

The second surgery was performed after the 8 weeks recovery period. General anesthesia and local infiltration anesthesia were performed as in the first surgery. A horizontal incision was made on the experimental site, and vertical incisions were made through the mucogingival junction that extended into the alveolar mucosa at the mesial and distal ends of each defect. The mucoperiosteal flaps were elevated to expose the edentulous alveolar ridge. Two identical dehiscence defects (4 mm apicocoronally and 2 mm mesiodistally) were surgically prepared on the buccal sides of the left and right partial edentulous ridges (figure 2). In each of the four defects, an implant was placed following serial drilling according to the standard protocol. The platform of the fixture was located at the level of the alveolar crest.

Next, 0.1 mg deproteinized bovine bone grafting material (Bio-Oss) was quantified and dampened in sterile saline for 5 min, then positioned at the buccal defect. Upon completion of the grafting, collagen membranes (Collagen Membrane, GENOSS) or PCL/PLGA/β-TCP membranes were randomly positioned at the buccal defect (figure 3). All membranes were cut to a size that covered 2–3 mm of the adjacent alveolar bone to overlap the entire defect. To enhance the stability of the grafting material, titanium pins (Dentium Co., Seoul, Korea) were used for the fixation. To obtain primary wound closure, the buccal flaps were carefully released and sutured. All surgeries were performed by the same professionally trained operator.

2.3.4. Post-operative care and sacrifice

Antibiotics such as penicillin G procaine and penicillin G benzathine were intramuscularly injected (1 ml/5 kg) immediately and 48 h after the surgery. Plaque was controlled using 2% chlorhexidine gluconate through daily flushing of the oral cavity until the end of the study. The animals were kept on a soft diet for 2 weeks, followed by a regular diet. Animals were sacrificed 8 weeks post-operatively through intravenous injection of concentrated sodium pentobarbital (Euthasol, Delmarva Laboratories Inc., Midlothian, VA, USA). The mandibles of the sacrificed beagles were harvested after cutting them to include the alveolar bones near the implant, as well as the membranes and surrounding mucosae. The 12 harvested mandible block sections were fixed using neutral buffered formalin (Sigma Aldrich).

2.3.5. Micro-computed tomography (μCT) analysis

After fixation, 3D μCT images were generated to analyze the new bone density and new bone volume of the peri-implant dehiscence defect area. The specimens were wrapped with Parafilm M® (Bemis Company, Inc., Neenah, Wisconsin, USA) to keep them from drying during the scanning process. Then, all the samples were scanned with 130 kV energy, 60 μA intensity, and a

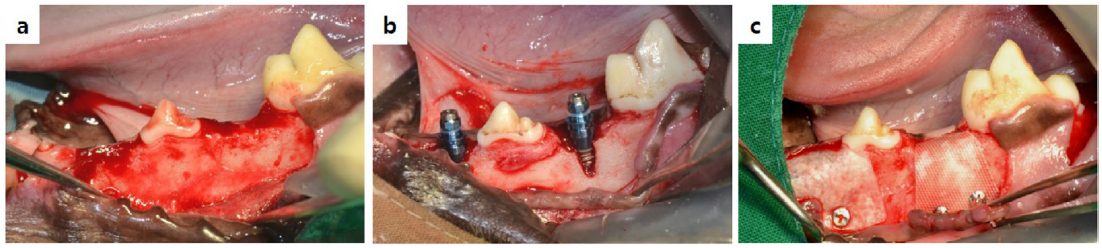

Figure 3. Surgical operation procedures. (a) The alveolar ridge was trimmed for implant insertion. (b) Buccal defects were created and implants were inserted into the partial edentulous mandibular alveolar ridge. (c) All the peri-implant defects were filled with the grafting material. Then, all the membranes were placed randomly on the defect.

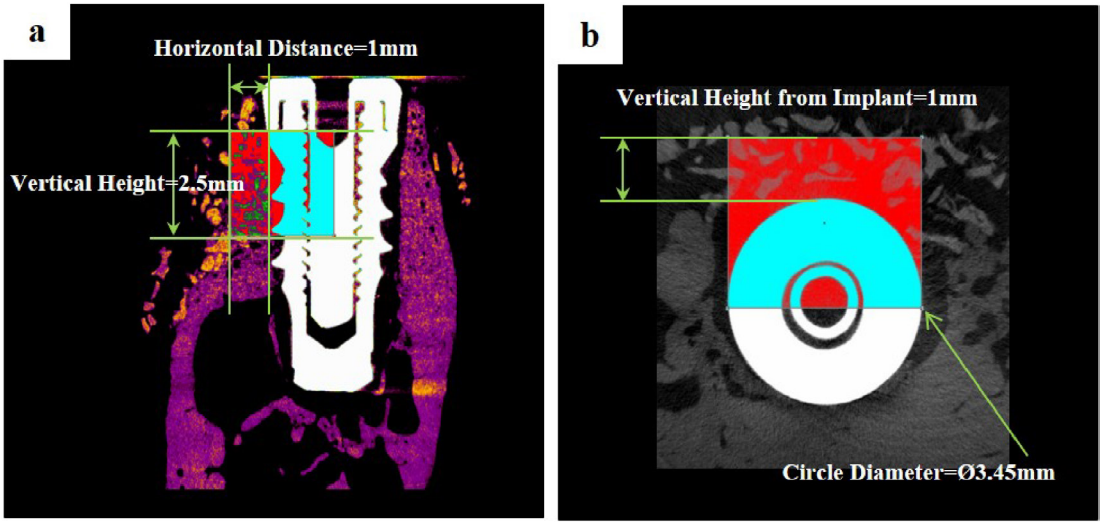

Figure 4. The region of interest; 1 mm in width and 2.5 mm in height from the implant platform. (a) Cross-sectional view (b) occlusal view.

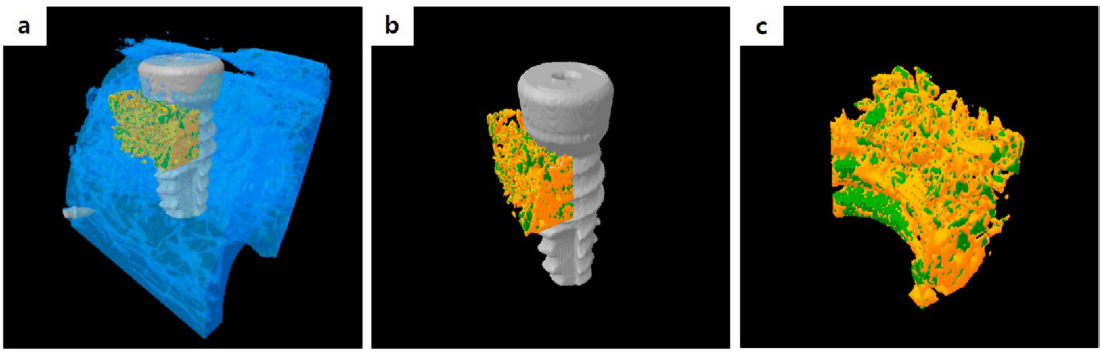

Figure 5. 3D images obtained via micro-computed tomography. (a) 3D image of the mandible block section. (b) 3D image without the old bone. (c) 3D image of the region of interest.

7.10 μm-pixel resolution using a bromine filter (0.25 mm) (Skyscan-1173, version 1.6, Bruker-CT, Kontich, Belgium). Reconstruction was performed using Nrecon software (version 1.6.10.1, Bruker-CT). All the applied scan and reconstruction parameters were identical for all the specimens. The overall augmented contour was evaluated at the 3D reconstructed view. Boundaries were set as follows to standardize the region of the augmented volume to be analyzed:

- Any augmented volume directly superior or lingual to the implant in its axial plane was excluded.
- Any augmented volume inferior to the buccal extension of the inferior border of the defect was excluded.

The region of interest (ROI) was 1 mm in width and 2.5 mm in height from the implant platform (figures 4 and 5).

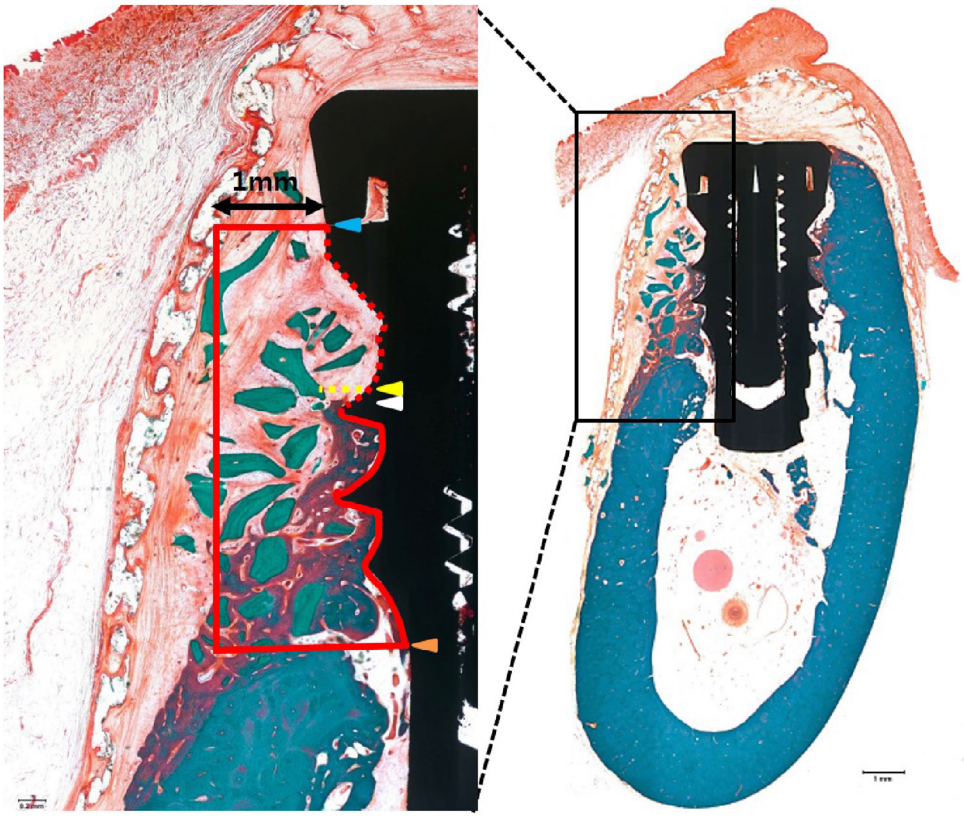

Figure 6. Parameters measured in the histologic specimens. Red box = area of interest. Blue arrow = platform of the implant. Yellow arrow = most coronal point of the new bone. White arrow = most coronal point of the osseointegration site. Green arrow = most coronal point of the old bone.

The following parameters were calculated within the ROI:

- Total augmented volume (TAV; mm^3)
: Area occupied by the total augmented volume within the ROI
- New bone volume (NBV; mm^3)
: Area occupied by the new bone volume within the ROI
- Remaining bone substitute volume (RBV; mm^3)
: Area occupied by the remaining bone substitute volume within the ROI
- Non-mineralized tissue volume (NMV; mm^3)
: Area occupied by the non-mineralized tissue volume within the ROI

2.3.6. Histomorphometric analysis

Upon completion of the μCT analysis, the specimens were cleansed and dehydrated using an ethanol series with increasing concentration. After the dehydration was completed, infiltration was conducted using a mixture of ethanol and Technovit 7200 resin (Heraeus Kulzer, Hanau, Germany) while increasing the resin ratio. Then the specimen was fixed on an embedding frame to perform embedding using a UV embedding system (Exakt 520, Kulzer) to cure the resin for 1 d. The polymerized specimen block was longitudinally sectioned at each implant center using the Exakt diamond cutting system (Kulzer Exakt 300 CP), and attached to slides using an adhesive press system. The final slides were ground to have a thickness ranging from the initial 400 μm to the final 40 $\pm$ 5 μm using the Exakt grinding system (Kulzer Exakt 400CS). To observe the newly regenerated bone in the specimen, Goldner Trichrome staining was conducted before mounting the sample, then final slides were prepared. The final slide images were captured using a CCD camera (Spot Insight 2 Mp scientific CCD digital camera system, Diagnostic Instruments, Inc., Sterling Heights, MI, USA) with an adaptor (U-CMA3, Olympus, Tokyo, Japan) mounted onto a light microscope coupled to a computer (BX51, Olympus). For the analysis of the captured images, i-Solution ver. 8.1 (IMT i-Solution, Inc., Coquitlam, BC, Canada) was used. The general specimen images were observed at $\times$12.5 magnification; for the histometric analyses, $\times$40 magnification was used. For the histometric analysis, a single, professionally trained and blinded investigator measured the following items.

The area of interest (AOI) was 1 mm width and height from the implant platform to the old bone (OB) (figure 6).

The following measurements were analyzed and recorded within the AOI.

- New bone area (NBA; %)
: Area occupied by the new bone/AOI $\times$ 100 (%)

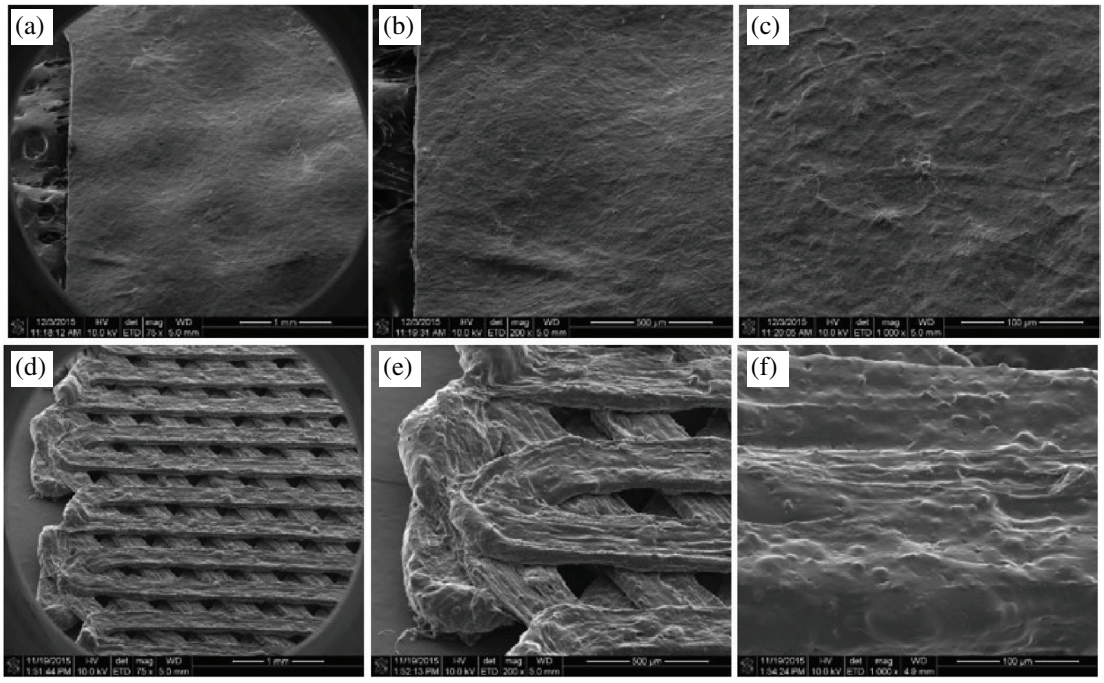

Figure 7. SEM images of collagen ((a)–(c)) and PCL/PLGA/β-TCP ((d)–(f)) membranes. Magnification, $\times$75 in ((a) and (d)), $\times$200 in ((b) and (e)) and $\times$1000 in ((c) and (f)). The collagen membrane showed a smooth surface without visible pore-like fabric, while the PCL/PLGA/β-TCP had a rough surface and a fully interconnected porous architecture.

Table 1. Maximum tensile load and elastic modulus of collagen and PCL/PLGA/β-TCP membranes under dry and wet condition (means $\pm$ SDs; $n = 3$).

	Maximum tensile load (N)		Elastic modulus (MPa)	
Group	Dry	Wet	Dry	Wet
Collagen	68.8 $\pm$ 15.3	12.8 $\pm$ 1.4	874.9 $\pm$ 87.3	7.9 $\pm$ 0.1
PCL/PLGA/β-TCP	15.7 $\pm$ 0.9	10.3 $\pm$ 0.9	803.0 $\pm$ 17.8	594.7 $\pm$ 66.7

- Remaining bone substitute area (RBA; %)
: Area occupied by the remaining bone substitute/AOI $\times$ 100 (%)
- Bone-to-implant contact (BIC; %)
: Length of the contact with the new bone/total length of the exposed threads $\times$ 100 (%)
- Bone crest (BC)-OB (%)
: Distance from the BC to the OB/distance from the implant platform to the OB $\times$ 100 (%)
- Coronal point of osseointegration (CO)-OB (%)
: Distance from the most CO to the OB/distance from the implant platform to the OB $\times$ 100 (%)

2.3.7. Statistical analysis

All the experimental data were expressed as the means, standard deviations, and medians. All the statistical analyses were conducted using software R (version 3.1.3). The treatment group (Collagen group and PCL/PLGA/β-TCP group) was set as an independent factor, and the dog number was set as a random factor. To compare the radiographic and histomorphmetric parameters of the groups, a non-parametric mixed model was used [41]. The statistical significance level was 5% and post hoc analyses were performed.

3. Results

3.1. SEM analysis of the PCL/PLGA/β-TCP membrane

Representative SEM images of the collagen and PCL/PLGA/β-TCP membranes are shown in figure 7. The surface of the collagen membrane was smooth and dense (figures 7(a)–(c)), whereas the PCL/PLGA/β-TCP surface was rough owing to the β-TCP particles. In particular, the PCL/PLGA/β-TCP membrane showed a triangular and uniform pore architecture that was fully interconnected (figures 7(d)–(f)).

3.2. Mechanical testing of collagen and PCL/PLGA/β-TCP membranes

To compare the mechanical properties of the PCL/PLGA/β-TCP membrane with those of the collagen membrane, a tensile test was performed under dry and wet conditions. The tensile test results of the collagen

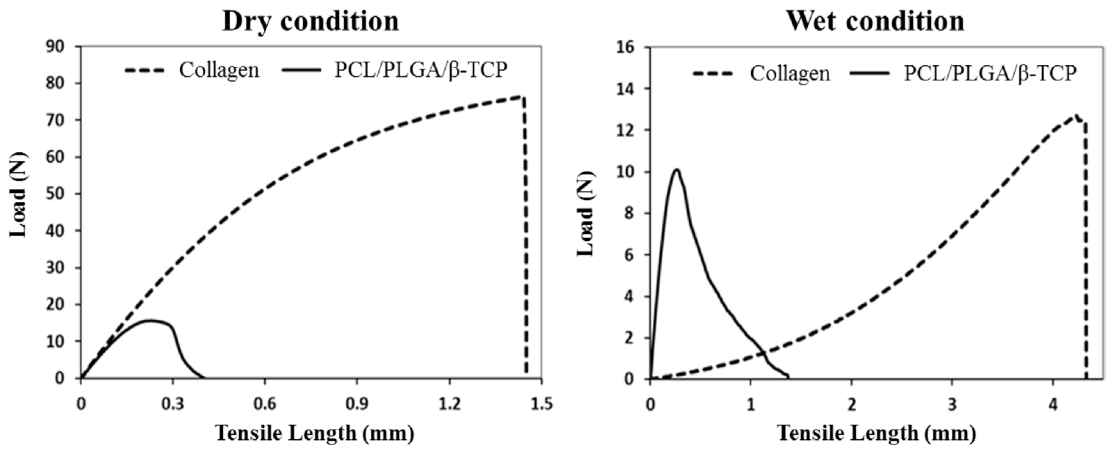

Figure 8. Tensile testing results (load-displacement curve) of collagen and PCL/PLGA/β-TCP membranes in the dry and wet conditions.

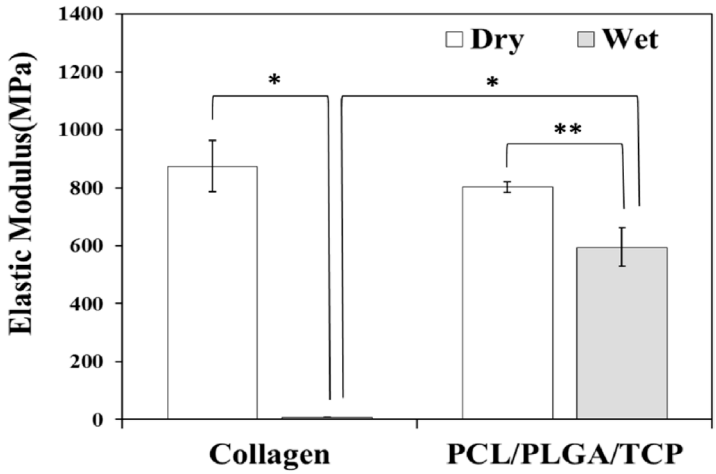

Figure 9. Elastic modulus of collagen and PCL/PLGA/β-TCP membranes in the dry and wet conditions ($^{*}P < 0.001$, $^{**}P < 0.01$). A substantial decrease of elastic modulus between dry and wet conditions was seen for the collagen membrane.

and PCL/PLGA/β-TCP membranes are shown in figures 8 and 9, and table 1. From the load-displacement curve (figure 8), the maximum load of the collagen membrane in the dry condition was approximately 4-times higher than that of the PCL/PLGA/β-TCP membrane. In contrast, in the wet condition, the maximum load of collagen (12.8 N) was 24.3% higher than that of PCL/PLGA/β-TCP membrane (10.3 N). On the other hand, as shown in figure 9, a considerable decrease of the elastic modulus (the slope of first linear portion of the stress–strain curve reflecting membrane rigidity) between the dry (874.9 ± 87.3 MPa) and wet (7.9 ± 0.1 MPa) conditions was measured in the collagen membrane ($P < 0.001$). Specifically, the elastic modulus of the collagen membrane in the dry condition fell by 99.1%. In contrast, that of the PCL/PLGA/β-TCP membrane in the dry condition decreased by 26% when the membrane was wetted ($P < 0.01$). Thus, the decreasing rate of the elastic modulus of the PCL/PLGA/β-TCP membrane in the wet condition was much less severe than that of the collagen membrane.

3.3. *In vitro* results

To evaluate the cytocompatibility of the membrane, we first observed the morphology and proliferation of fibroblasts (NIH3T3) and preosteoblasts (MC3T3-E1 cells) seeded onto the membranes. On day 2, the number of attached cells on the collagen membrane was approximately 2.6-times higher than that on PCL/PLGA/β-TCP for both cell types. However, proliferation of the MC3T3-E1 cells on PCL/PLGA/β-TCP increased and had reached similar levels as that on the collagen membrane by day 4 ($P > 0.05$). In parallel, SEM images showed that the MC3T3 cells completely covered the surface of the collagen and PCL/PLGA/β-TCP membranes on day 7 (figure 10(b)). On the other hand, the optical density of NIH3T3 cells did not differ between membrane type ($P > 0.05$) at day 7 even though it had retained a significant difference up to 4 d ($P < 0.001$) (figure 10(a)). These results suggested that the PCL/PLGA/β-TCP membrane provide an appropriate environment for cell proliferation.

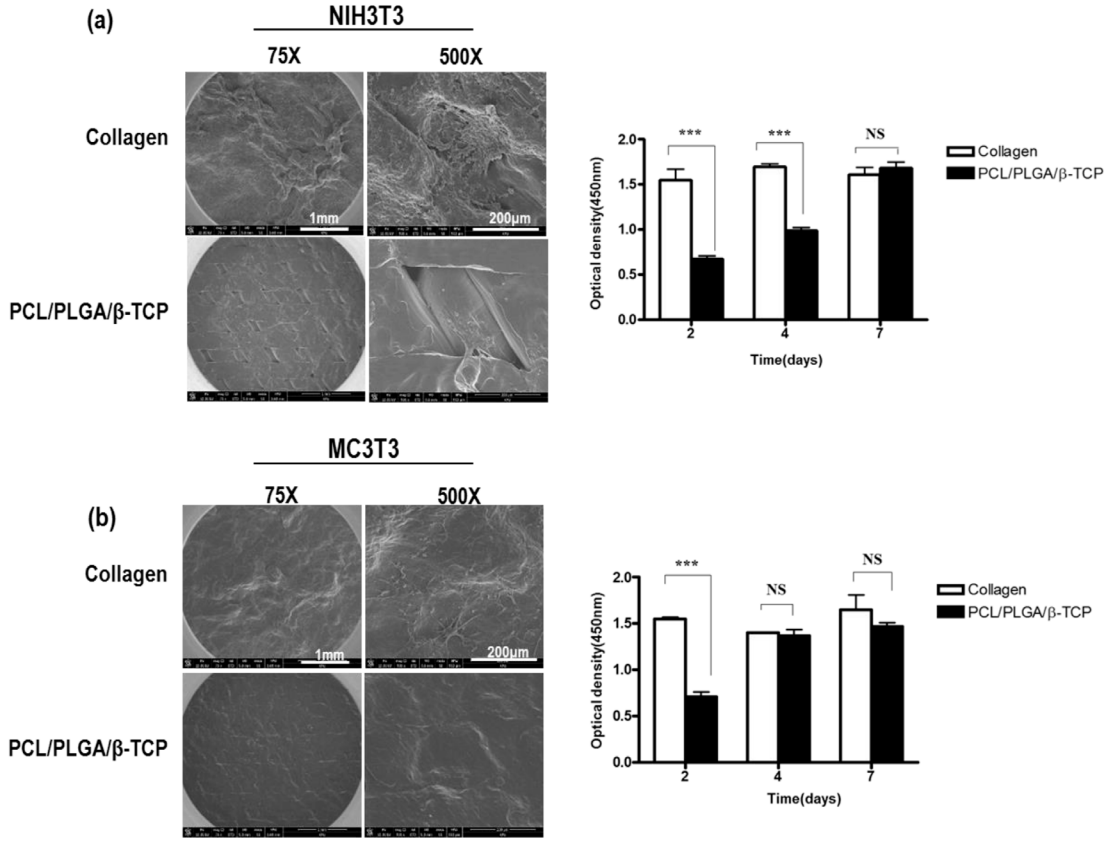

Figure 10. The cell morphology and proliferation assays of NIH3T3 (a) and MC3T3-E1 (b) cells on the collagen and PCL/PLGA/β-TCP membranes showed that the attached cells grew well. (***$P < 0.001$, NS = no significant difference).

We further investigated the osteogenic differentiation of MC3T3-E1 cells on collagen and PCL/PLGA/β-TCP membranes. The MC3T3-E1-seeded membranes were placed in osteogenic media for 7 and 14 d and then fixed with 4% paraformaldehyde. Osteogenic differentiation of the MC3T3-E1 cells on the membranes was assessed by alizarin red S staining, which revealed increased calcium deposition on the membranes (figure 11(a)). To quantify the staining, stained dyes were extracted from the membranes using 10% cetylpyridinium chloride in 10 mM sodium phosphate. On day 7, the level of osteogenic differentiation of MC3T3-E1 cells on the PCL/PLGA/β-TCP membrane was less than that on the collagen membrane. However, no significant difference between membrane type could be determined on day 14. The quantitative analysis results were consistent with the staining results (figure 11(b)). Taken together, the *in vitro* experiments demonstrated that the PCL/PLGA/β-TCP membrane exhibited similar efficacy as a GBR membrane with respect to cytocompatibility and osteogenic differentiation as compared to collagen.

3.4. *In vivo* results

3.4.1. *Clinical findings*

All experimental animals survived the surgical procedures, and the 12 implant sites healed without noted problems. No implant failure or dropout was observed, and no membrane exposure or separation occurred during the healing period. No complication was reported from either experimental group during the study period.

3.4.2. *Volumetric analysis using μCT*

In the collagen group, some specimens were observed wherein the grafting materials were scattered in the peri-implant dehiscence defect area. In comparison, in the PCL/PLGA/β-TCP group, the grafting materials formed a shape in the peri-implant dehiscence defect area in most specimens (figure 12).

The volumetric measurements are summarized in table 2 and figure 13. The PCL/PLGA/β-TCP group showed higher levels of new bone volume (mm^3) and remaining bone substitute volume (mm^3) than the collagen group, but the differences were statistically insignificant (NBV (mm^3), $P = 0.339$; and RBV (mm^3), $P = 0.295$). Conversely, the collagen group showed higher levels of total augmented volume (mm^3) and non-mineralized tissue volume (mm^3) than the PCL/PLGA/β-TCP group, but the differences were also statistically insignificant (TAV (mm^3). $P = 0.127$; and NMV (mm^3), $P = 0.185$).

3.4.3. *Histologic findings*

In the collagen group (figure 14), a small amount of new bone was formed in the implant in the buccal peri-implant dehiscence defect area. In some specimens, the membrane was not observed because it was absorbed. In the specimen whose membrane was completely absorbed,

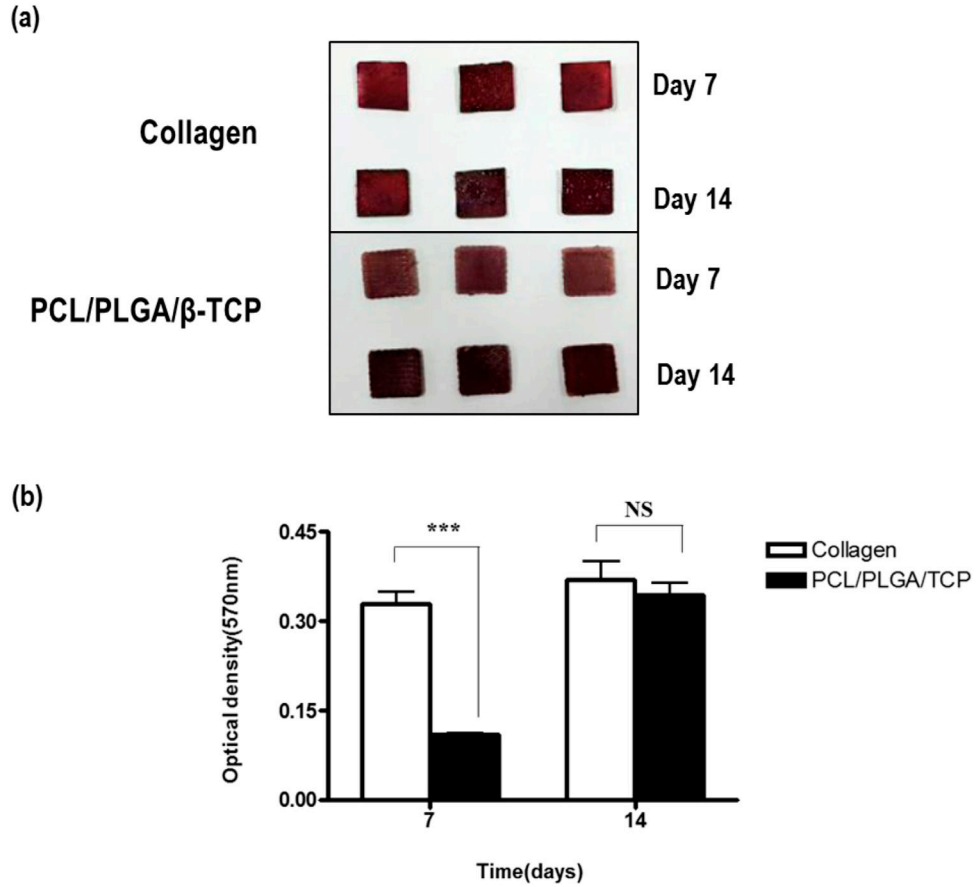

Figure 11. Alizarine red S staining (a) and quantification (b) indicated that no difference was observed in osteogenic differentiation between collagen and PCL/PLGA/β-TCP membranes at day 14.

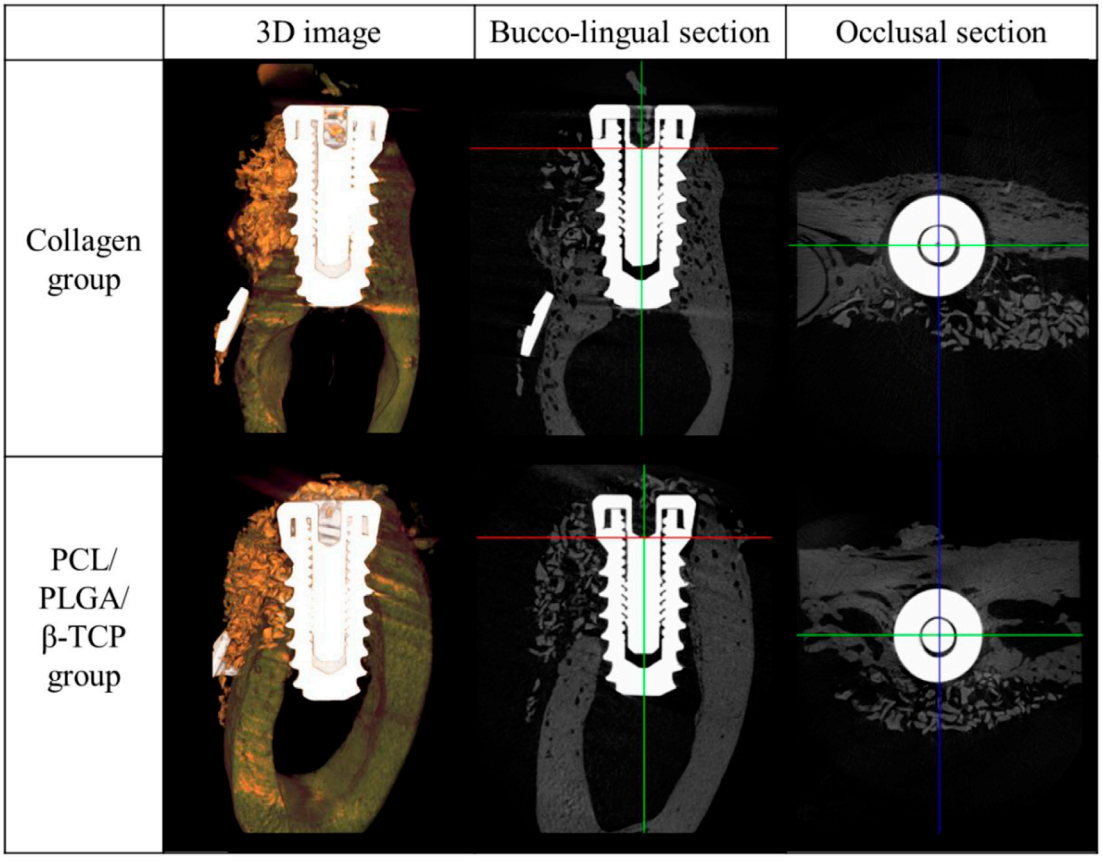

Figure 12. Micro-computed tomography images of the collagen and PCL/PLGA/β-TCP groups.

Table 2. Volumetric analysis within the area of interest ($n = 6$; mm^3).

	NBV (mm^3)	TAV (mm^3)	RBV (mm^3)	NMV (mm^3)
Collagen				
Mean ± SD	1.28 ± 0.70	14.27 ± 0.19	2.69 ± 1.97	10.29 ± 2.71
Median	0.98	14.27	1.88	11.42
PCL/PLGA/β-TCP				
Mean ± SD	1.57 ± 0.70	14.04 ± 0.31	3.95 ± 1.97	8.52 ± 2.47
Median	1.56	14.05	4.15	8.23
P	0.339	0.127	0.295	0.185

Note: NBV, new bone volume; TAV, total augmented volume; RBV, remaining bone substitute volume; NMV, non-mineralized tissue volume.
No significant difference between the two experiment groups ($P > 0.05$).

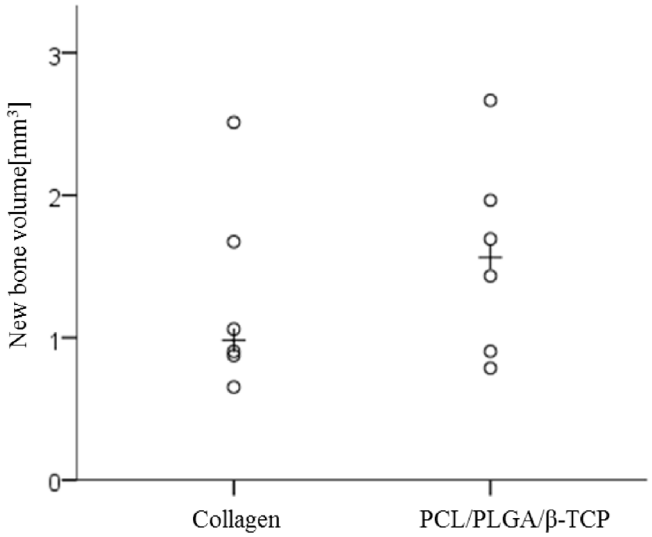

Figure 13. Scatter plot and median (plus sign) representing the new bone volume (mm^3).

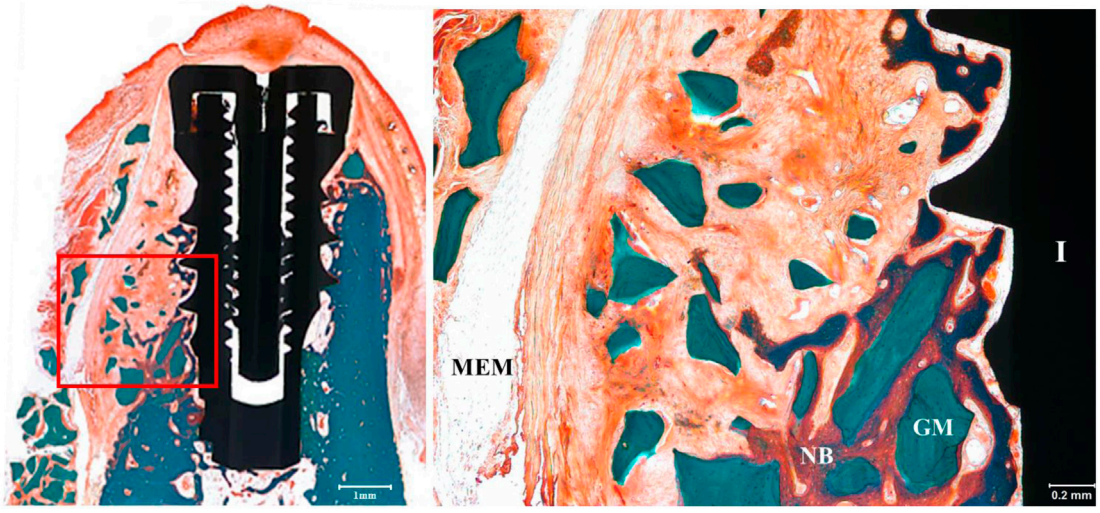

Figure 14. Histological sections of the collagen group. A small amount of new bone was formed. NB, new bone; GM, grafting material; MEM, membrane; I, implant (Goldner Trichrome stain; magnification ×12.5 (a) and ×40 (b)).

fibrous tissues were observed around the implant, and the grafting materials were observed only because they were scattered in the peri-implant dehiscence defect area.

In the PCL/PLGA/β-TCP group (figure 15), a comparatively large amount of new bone was formed in the implant in the buccal peri-implant dehiscence defect area. The membranes survived in most of the specimens, and a large amount of the grafting material that formed a shape was observed in the peri-implant dehiscence defect area.

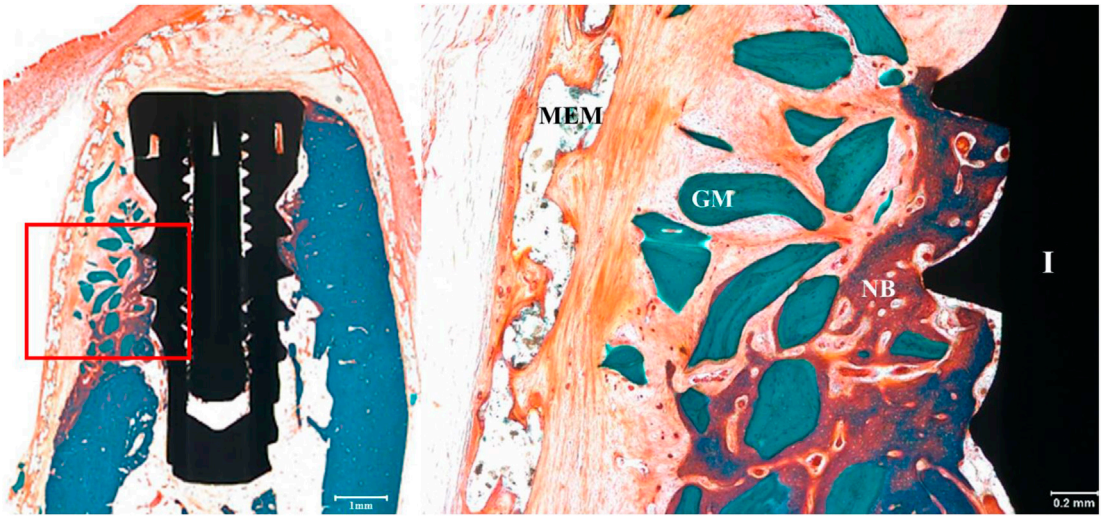

Figure 15. Histological sections of the PCL/PLGA/β-TCP group. A large amount of new bone was formed. NB, new bone; GM, grafting material; MEM, membrane; I, implant (Goldner Trichrome stain; magnification $\times$12.5 (a) and $\times$40 (b)).

Table 3. Histometric analysis within the area of interest ($n = 6$; %).

	NBA (%)	RBA (%)	BIC (%)	BC-OB (%)	CO-OB (%)
Collagen					
Mean $\pm$ SD	13.84 $\pm$ 4.60	16.08 $\pm$ 3.25	40.22 $\pm$ 10.71	55.81 $\pm$ 9.41	47.03 $\pm$ 10.19
Median	12.86	15.69	38.00	52.70	46.15
PCL/PLGA/β-TCP					
Mean $\pm$ SD	24.36 $\pm$ 3.90	19.19 $\pm$ 5.28	56.48 $\pm$ 4.68	57.11 $\pm$ 6.08	51.59 $\pm$ 8.51
Median	24.07	18.37	57.63	58.69	52.62
P	0.000[a]	0.256	0.000[a]	0.759	0.185

[a]Indicates statistical significance between the two experiment groups ($P < 0.05$).
Note: NBA, new bone area; RBA, remaining bone substitute area; BIC, bone-to-implant contact; BC-OB, distance from the bone crest to the old bone; CO-OB, distance from the most coronal point of the osseointegration to the old bone.

3.4.4. *Histometric analysis*

The histometric measurements are summarized in table 3 and figure 16. The PCL/PLGA/β-TCP group showed significantly higher levels than the collagen group. In terms of the new bone area and the bone-to-implant contact; (NBA (%), $P = 0.000$; and BIC (%), $P = 0.000$). The PCL/PLGA/β-TCP group also showed higher levels of the collagen group in terms of the remaining bone substitute area (%), BC-OB (%) and CO-OB (%), but the difference was insignificant (RBA (%), $P = 0.256$; BC-OB (%), $P = 0.759$; and CO-OB (%), $P = 0.185$).

4. Discussion

GBR maintains the defect area after the extraction of a tooth before an implant, enhancing the migration of surrounding bone tissue and preventing ingrowth of soft tissue [42]. GBR is removed approximately 3–4 months after surgery when the bone is reconstructed and ready for an implant. For these reasons, first, GBR membranes must be biocompatible to allow migration and proliferation of the surrounding tissue. In addition, GBR membranes must be able to protect the wound area from mechanical disruption and salivary contamination and must be naturally resorbed so that an additional surgery is not required for their removal [43–45]. Collagen membranes have gained popularity as a GBR membrane as they facilitate cell attachment and proliferation in the defect area, resulting in effective bone formation, are bioresorbable within 4 weeks after the application, which obviates a second surgery for removal, and have little immunogenicity [18, 22, 46, 47]. Hence, for comparison with collagen membranes, this study fabricated 3D-printed PCL/PLGA/β-TCP membranes using a combination of TCP, a biodegradable material known to induce bone formation by releasing calcium, and two biocompatible polymers, PCL and PLGA [37, 38].

Synthetic biomaterials such as PCL, poly lactic acid, poly glycolic acid, and PLGA have been used to prepare the scaffolds for enhanced tissue regeneration [36]. In particular, PLGA is used for the reconstruction of various tissues owing to its high cytocompatibility [36, 48, 49].

However, scaffolds composed only of PLGA do not maintain their shapes either in the *in vitro* or *in vivo* environments owing to their brittle property and rapid

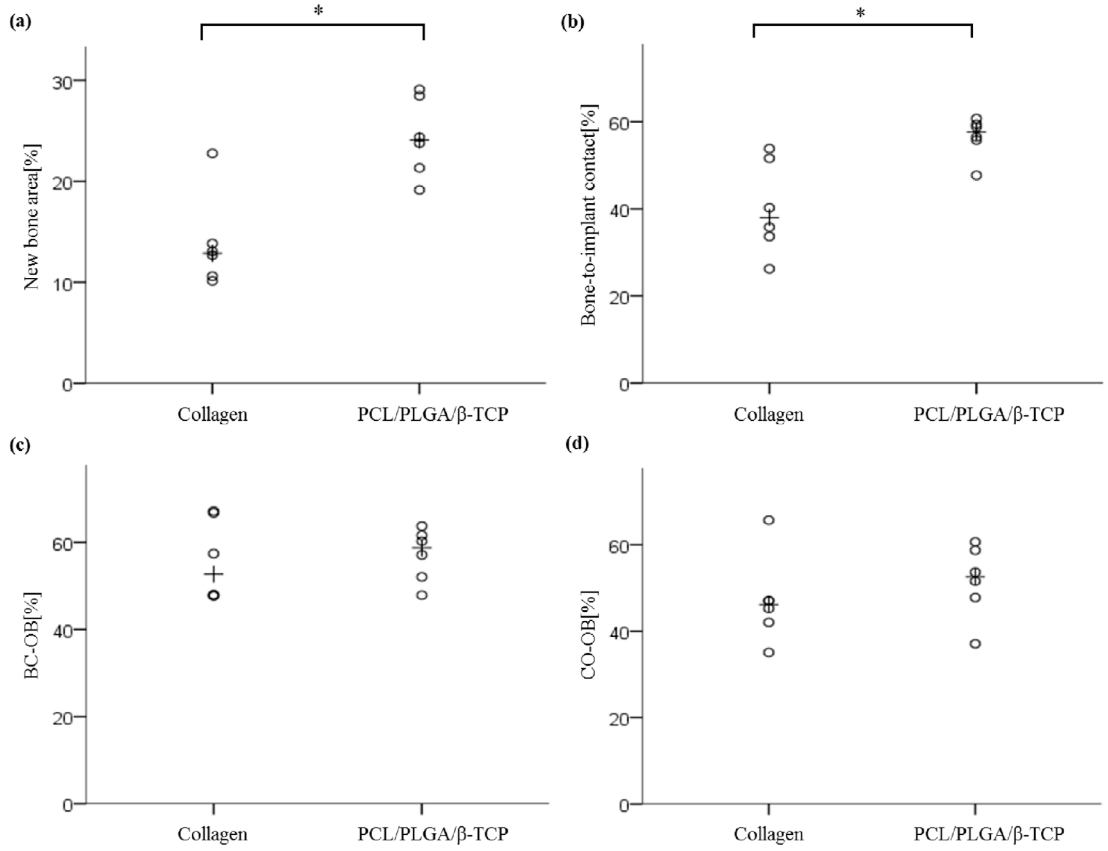

Figure 16. Scatter plot and median (plus sign) representing (a) the new bone area, (b) bone-to-implant contact within the defect, (c) distance from the bone crest to the old bone, and (d) distance from the most coronal point of the osseointegration to the old bone ($n = 6$). *Significantly different ($P < 0.05$).

resorption [34, 50]. In contrast, PCL has comparatively less cell affinity than PLGA, but it has excellent mechanical properties that prevent early fractures of the scaffold [39] and its degradation rate is slower than the rate of bone regeneration [51]. Thus, blended PCL/PLGA scaffolds exhibit biological and mechanical advantages obtained during the PCL and PLGA mixing processes that complement their respective weaknesses [36]. In addition, as β-TCP was added to the blended PCL/PLGA for the fabrication of the PCL/PLGA/β-TCP membrane, their elastic modulus was enhanced and their surface roughness was increased [1, 52, 53]. In the SEM images of the PCL/PLGA/β-TCP membranes prepared in this study, the rough surfaces generated by the incorporated β-TCP were confirmed (figure 7). During cellular testing with fibroblasts and preosteoblasts, early cell attachment and differentiation were higher in collagen, but the difference of proliferation and differentiation had disappeared when examined on day 7 and day 14, respectively. In contrast, fibroblasts aggregated and were detached from the membrane when maintained until day 14 (data not shown). This was in line with the results of a previous paper [40] and is an indication of the membrane's ability to inhibit the ingrowth of soft tissues.

We next applied the GBR to an *in vivo* implant model utilizing beagle dogs and performed histological analyses after sacrifice at 8 weeks. The histologic and histomorphometric analyses in this study showed that the PCL/PLGA/β-TCP group did not differ significantly from the collagen group; furthermore, in particular among the histometric measurements, the new bone area (%) and bone-to implant contact (%) of the PCL/PLGA/β-TCP group were significantly higher than those of the collagen group ($P < 0.05$). These findings indicated that the group receiving PCL/PLGA/β-TCP membranes showed levels of new bone formation and regeneration in the defect area comparable with those induced by collagen membranes, confirming that the biocompatibility of the PCL/PLGA/β-TCP membranes as well as their ability to maintain migration and proliferation of surrounding tissue and to support osteogenic differentiation to ultimately induce bone formation are comparable to those of collagen.

Rakhmatia *et al* [9] suggested that a non-resorbable titanium mesh could be an excellent solution when special mechanical support is required for bone defect treatments. According to Hämmerle & Jung [13], a titanium-reinforced e-PTFE membrane can be used in GBR for large defects; on the other hand, in casual dehiscence defect cases, the resorbable membrane is the current material of choice. However, in response to a report that resorbable membranes such as collagen have disadvantages as barriers owing to inferior generation of implant space caused by their poor mechanical properties [12], we performed mechanical property testing

for PCL/PLGA/β-TCP membranes under biomimetic dry and wet conditions. As shown in figures 8 and 9, and table 1, the elastic modulus of collagen markedly decreased in dry and wet conditions whereas that of the PCL/PLGA/β-TCP membrane was relatively stable. Furthermore, in the volumetric analysis using μCT, the PCL/PLGA/β-TCP group showed a greater new bone volume (mm^3) than the collagen group. This might have been due to the stability of the PCL/PLGA/β-TCP membrane based on its superior mechanical properties and slower degradation rate. This finding shows that PCL/PLGA/β-TCP membranes are stable in maintaining their structure and during the space-making required for bone regeneration in defect areas exposed to blood, saliva, and irrigation, which would be a beneficial property for use as a GBR membrane.

In addition, the PCL/PLGA/β-TCP membrane can be prepared quickly and economically using 3D printing technology to generate diverse shapes, thicknesses, pore sizes, pore geometries, and porosities. Upon loading antibiotics, growth factors, or adhesion factors, this synthetic membrane can be used as a delivery device for specific agents [38, 54]. In addition, its mechanical properties and degradation rate can be modified according to the component ratio. Actually, in the previously study, we combined PCL/PLGA/β-TCP in a ratio of 2:6:2, to manufacture a membrane that would reflect the stiff properties of PLGA with the focusing physical strength like titanium membrane [39, 40]. In the present experiment, PCL/PLGA/β-TCP was combined in a ratio of 4:5:1. Increasing the proportion of PCL aims to make the membrane flexible, like a collagen membrane, while also acquiring a little space maintaining ability. Therefore, the membranes used in this study were much softer than those used in the previous study [40], and we could bended and shaped membranes to fit the patient's defect, ultimately maintaining the space for bone regeneration. It will be also helpful to maintain the bone grafting materials within defect area. We concluded from this study that this membrane is more effective in handling and maintaining the space while it also embraces the advantages of collagen membrane such as resorption, biocompatibility and barrier function.

Overall, our results demonstrate that the 3D-printed PCL/PLGA/β-TCP membrane is useful as a GBR membrane. In addition, it can be prepared in the form of a patient-specific membrane from personal CT scan data, and it can be fabricated as a drug- or growth factor-releasing bioactive membrane. Further studies will likely be required to define and optimize these and other potential future uses.

5. Conclusions

In this study, the 3D-printed PCL/PLGA/β-TCP membrane showed a bone regeneration performance similar to that of collagen membranes during a GBR procedure performed in peri-implant defects. Therefore, the 3D-printed PCL/PLGA/β-TCP membrane was confirmed to have substantial efficacy as a resorbable GBR membrane for peri-implant defect treatment. Considering the higher stability of membrane, the 3D-printed PCL/PLGA/β-TCP membrane is expected to become a feasible alternative to the commonly utilized collagen membrane.

Acknowledgments

This research was supported by a grant from the Korean Health Technology R&D Project through the Korean Health Industry Development Institute (KHIDI), funded by the Korean Ministry of Health & Welfare (grant number: HI14C3309).

Conflicts of interest

The authors declare no conflict of interest.

References

[1] Chiapasco M and Zaniboni M 2009 Clinical outcomes of GBR procedures to correct peri-implant dehiscences and fenestrations: a systematic review *Clin. Oral Implants Res.* **20** 113–23
[2] Maghaireh H, Saad M and Assaf A 2012 Guided bone regeneration: evidence and limits *Smile Dent. J.* **7** 8–16
[3] Ilizarov G A 1989 The tension-stress effect on the genesis and growth of tissues: part I. The influence of stability of fixation and soft-tissue preservation *Clin. Orthop. Relat. Res.* **238** 249–81
[4] Reddi A, Wientroub S and Muthukumaran N 1987 Biologic principles of bone induction *Orthop. Clin. North Am.* **18** 207
[5] Burchardt H 1983 The biology of bone graft repair *Clin. Orthop. Related Res.* **174** 28–34
[6] Hämmerle C H and Karring T 1998 Guided bone regeneration at oral implant sites *Periodontology 2000* **17** 151–75
[7] Chiapasco M, Casentini P and Zaniboni M 2009 Bone augmentation procedures in implant dentistry *Int. J. Oral Maxillofac. Implants* **24** 237–59
[8] Hämmerle C H, Jung R E and Feloutzis A 2002 A systematic review of the survival of implants in bone sites augmented with barrier membranes (guided bone regeneration) in partially edentulous patients *J. Clin. Periodontol.* **29** 226–31
[9] Rakhmatia Y D, Ayukawa Y, Furuhashi A and Koyano K 2013 Current barrier membranes: titanium mesh and other membranes for guided bone regeneration in dental applications *J. Prosthodont. Res.* **57** 3–14
[10] Dahlin C, Sennerby L, Lekholm U, Linde A and Nyman S 1989 Generation of new bone around titanium implants using a membrane technique: an experimental study in rabbits *Int. J. Oral Maxillof. Implants* **4** 19–25
[11] Scantlebury T V 1993 1982–1992: a decade of technology development for guided tissue regeneration *J. Periodontol.* **64** 1129–37
[12] Liu J and Kerns D G 2014 Suppl 1: mechanisms of guided bone regeneration: a review *Open Dent. J.* **8** 56
[13] Hämmerle C H and Jung R E 2003 Bone augmentation by means of barrier membranes *Periodontology 2000* **33** 36–53
[14] Gentile P, Chiono V, Tonda-Turo C, Ferreira A M and Ciardelli G 2011 Polymeric membranes for guided bone regeneration *Biotechnol. J.* **6** 1187–97
[15] Simion M, Baldoni M, Rassi P and Zaffe D 1994 A comparative study of the effectiveness of e-PTFE membranes with and without early exposure during the healing period *Int. J. Periodontics Restorative Dent.* **14** 166–80

[16] Parodi R, Carusi G, Santarelli G and Nanni F 1998 Implant placement in large edentulous ridges expanded by GBR using a bioresorbable collagen membrane *Int. J. Periodontics Restorative Dent.* **18** 266–75
[17] Hämmerle C H and Lang N P 2001 Single stage surgery combining transmucosal implant placement with guided bone regeneration and bioresorbable materials *Clin. Oral Implants Res.* **12** 9–18
[18] Postlethwaite A E, Seyer J M and Kang A H 1978 Chemotactic attraction of human fibroblasts to type I, II, and III collagens and collagen-derived peptides *Proc. Natl Acad. Sci.* **75** 871–5
[19] Hürzeler M B, Kohal R J, Naghshbandl J, Mota L F, Conradt J, Hutmacher D and Caffesse R G 1998 Evaluation of a new bioresorbable barrier to facilitate guided bone regeneration around exposed implant threads: an experimental study in the monkey *Int. J. Oral Maxillof. Surg.* **27** 315–20
[20] Miller N, Penaud J, Foliguet B, Membre H, Ambrosini P and Plombas M 1996 Resorption rates of 2 commercially available bioresorbable membranes *J. Clin. Periodontol.* **23** 1051–9
[21] Zhao S, Pinholt E M, Madsen J E and Donath K 2000 Histological evaluation of different biodegradable and non-biodegradable membranes implanted subcutaneously in rats *J. CranioMaxillof. Surg.* **28** 116–22
[22] Owens K W and Yukna R A 2001 Collagen membrane resorption in dogs: a comparative study *Implant Dent.* **10** 49–58
[23] Hämmerle C H, Olah A J, Schmid J, Gogolewski S, Winkler J R and Lang N P 1997 The biological effect of natural bone mineral on bone neoformation on the rabbit skull *Clin. Oral Implants Res.* **8** 198–207
[24] Hutmacher D, Hürzeler M B and Schliephake H 1996 A review of material properties of biodegradable and bioresorbable polymers and devices for GTR and GBR applications *Int. J. Oral Maxillof. Implants* **11** 667–78
[25] Lundgren D, Sennerby L, Falk H, Friberg B and Nyman S 1994 The use of a new bioresorbable barrier for guided bone regeneration in connection with implant installation. Case reports *Clin. Oral Implants Res.* **5** 177–84
[26] Lundgren A, Sennerby L, Lundgren D, Taylor A, Gottlow J and Nyman S 1997 Bone augmentation at titanium implants using autologous bone grafts and a bioresorbable barrier. An experimental study in the rabbit tibia *Clin. Oral Implants Res.* **8** 82–9
[27] Lundgren A, Lundgren D, Sennerby L, Taylor Å, Gottlow J and Nyman S 1997 Augmentation of skull bone using a bioresorbable barrier supported by autologous bone grafts. An intra-individual study in the rabbit *Clin. Oral Implants Res.* **8** 90–5
[28] Lekovic V, Camargo P M, Klokkevold P R, Weinlaender M, Kenney E B, Dimitrijevic B and Nedic M 1998 Preservation of alveolar bone in extraction sockets using bioabsorbable membranes *J. Periodontol.* **69** 1044–9
[29] Hua N, Ti V L and Xu Y 2014 Biodegradable effect of PLGA membrane in alveolar bone regeneration on beagle dog *Cell Biochem. Biophys.* **70** 1051–5
[30] Loh Q L and Choong C 2013 Three-dimensional scaffolds for tissue engineering applications: role of porosity and pore size *Tissue Eng.* B **19** 485–502
[31] Shim J-H, Huh J-B, Park J Y, Jeon Y-C, Kang S S, Kim J Y, Rhie J-W and Cho D-W 2012 Fabrication of blended polycaprolactone/poly (lactic-co-glycolic acid)/β-tricalcium phosphate thin membrane using solid freeform fabrication technology for guided bone regeneration *Tissue Eng.* A **19** 317–28
[32] Lin C Y, Kikuchi N and Hollister S J 2004 A novel method for biomaterial scaffold internal architecture design to match bone elastic properties with desired porosity *J. Biomech.* **37** 623–36
[33] Hutmacher D W, Sittinger M and Risbud M V 2004 Scaffold-based tissue engineering: rationale for computer-aided design and solid free-form fabrication systems *Trends Biotechnol.* **22** 354–62
[34] Kim J Y, Park E K, Kim S-Y, Shin J-W and Cho D-W 2008 Fabrication of a SFF-based three-dimensional scaffold using a precision deposition system in tissue engineering *J. Micromech. Microeng.* **18** 055027
[35] Kim J Y, Jin G-Z, Park I S, Kim J-N, Chun S Y, Park E K, Kim S-Y, Yoo J, Kim S-H and Rhie J-W 2010 Evaluation of solid free-form fabrication-based scaffolds seeded with osteoblasts and human umbilical vein endothelial cells for use *in vivo* osteogenesis *Tissue Eng.* A **16** 2229–36
[36] Kim J Y, Yoon J J, Park E K, Kim D S, Kim S-Y and Cho D-W 2009 Cell adhesion and proliferation evaluation of SFF-based biodegradable scaffolds fabricated using a multi-head deposition system *Biofabrication* **1** 015002
[37] Shim J-H, Moon T-S, Yun M-J, Jeon Y-C, Jeong C-M, Cho D-W and Huh J-B 2012 Stimulation of healing within a rabbit calvarial defect by a PCL/PLGA scaffold blended with TCP using solid freeform fabrication technology *J. Mater. Sci., Mater. Med.* **23** 2993–3002
[38] Shim J-H, Yoon M-C, Jeong C-M, Jang J, Jeong S-I, Cho D-W and Huh J-B 2014 Efficacy of rhBMP-2 loaded PCL/PLGA/β-TCP guided bone regeneration membrane fabricated by 3D printing technology for reconstruction of calvaria defects in rabbit *Biomed. Mater.* **9** 065006
[39] Shim J-H, Kim J Y, Park M, Park J and Cho D-W 2011 Development of a hybrid scaffold with synthetic biomaterials and hydrogel using solid freeform fabrication technology *Biofabrication* **3** 034102
[40] Shim J-H, Won J-Y, Sung S-J, Lim D-H, Yun W-S, Jeon Y-C and Huh J-B 2015 Comparative efficacies of a 3D-printed PCL/PLGA/β-TCP membrane and a titanium membrane for guided bone regeneration in beagle dogs *Polymers* **7** 2061–77
[41] Brunner E and Langer F 2000 Nonparametric analysis of ordered categorical data in designs with longitudinal observations and small sample sizes *Biom. J.* **42** 663–75
[42] Lekovic V, Klokkevold P R, Kenney E B, Dimitrijelic B, Nedic M and Weinlaender M 1998 Histologic evaluation of guided tissue regeneration using 4 barrier membranes: a comparative furcation study in dogs *J. Periodontol.* **69** 54–61
[43] Hardwick R and Dahlin C 1994 Healing pattern of bone regeneration in membrane-protected defects: a histologic study in the canine mandible *Int. J. Oral Maxillof. Implants* **9** 13–29
[44] Javed A, Chen H and Ghori F Y 2010 Genetic and transcriptional control of bone formation *Oral Maxillof. Surg. Clin. North Am.* **22** 283–93
[45] Quilligan G 2010 20 years of guided bone regeneration in implant dentistry *Br. Dent. J.* **209** 192
[46] Wang H-L and Carroll W J 2001 Guided bone regeneration using bone grafts and collagen membranes *Quintessence Int.* **32** 504–15
[47] Schlegel A, Möhler H, Busch F and Mehl A 1997 Preclinical and clinical studies of a collagen membrane (Bio-Gide®) *Biomaterials* **18** 535–8
[48] Tang Z, Callaghan J and Hunt J 2005 The physical properties and response of osteoblasts to solution cast films of PLGA doped polycaprolactone *Biomaterials* **26** 6618–24
[49] Kim M S, Ahn H H, Shin Y N, Cho M H, Khang G and Lee H B 2007 An *in vivo* study of the host tissue response to subcutaneous implantation of PLGA-and/or porcine small intestinal submucosa-based scaffolds *Biomaterials* **28** 5137–43
[50] Shim J-H, Kim J Y, Park J K, Hahn S K, Rhie J-W, Kang S-W, Lee S-H and Cho D-W 2010 Effect of thermal degradation of SFF-based PLGA scaffolds fabricated using a multi-head deposition system followed by change of cell growth rate *J. Biomater. Sci.* **21** 1069–80
[51] Sun H, Mei L, Song C, Cui X and Wang P 2006 The *in vivo* degradation, absorption and excretion of PCL-based implant *Biomaterials* **27** 1735–40
[52] Oh S, Oh N, Appleford M and Ong J L 2006 Bioceramics for tissue engineering applications—a review *Am. J. Biochem. Biotechnol.* **2** 49–56
[53] Li X, van Blitterswijk C A, Feng Q, Cui F and Watari F 2008 The effect of calcium phosphate microstructure on bone-related cells *in vitro Biomaterials* **29** 3306–16
[54] Sam G and Pillai B R M 2014 Evolution of barrier membranes in periodontal regeneration-are the third generation membranes really here? *J. Clin. Diagn. Res.* **8** ZE14